OPTICS

Highly multicolored light-emitting arrays for compressive spectroscopy

Vivian Wang[1,2], Shiekh Zia Uddin[1,2], Junho Park[1,2], Ali Javey[1,2]*

Miniaturized, multicolored light-emitting device arrays are promising for applications in sensing, imaging, computing, and more, but the range of emission colors achievable by a conventional light-emitting diode is limited by material or device constraints. In this work, we demonstrate a highly multicolored light-emitting array with 49 different, individually addressable colors on a single chip. The array consists of pulsed-driven metal-oxide-semiconductor capacitors, which generate electroluminescence from microdispensed materials spanning a diverse range of colors and spectral shapes, enabling facile generation of arbitrary light spectra across a broad wavelength range (400 to 1400 nm). When combined with compressive reconstruction algorithms, these arrays can be used to perform spectroscopic measurements in a compact manner without diffractive optics. As an example, we demonstrate microscale spectral imaging of samples using a multiplexed electroluminescent array in conjunction with a monochrome camera.

INTRODUCTION

Although multicolored light-emitting arrays are valuable in many areas, including low-power sensing, computing, and spectroscopy (*1*–*3*), the spectral range of light-emitting devices integrated on a single chip is typically limited to no more than a few colors. Among the most ubiquitous examples of multicolor light-emitting device arrays are displays, which integrate red, green, and blue light-emitting diodes (LEDs) to produce a wide color gamut (*4*). Although light-emitting device arrays with a greater number of colors and broader spectral range are useful for multispectral sensing, lattice matching requirements limit the breadth of inorganic materials and thus bandgaps that can be grown on a single substrate (*5*). Commercial multiwavelength LED packages instead integrate devices fabricated on separate chips, which results in large package sizes relative to the size of individual devices. Organic materials can be integrated more readily on a single chip because of less demanding growth requirements, but such an approach is cost prohibitive from a manufacturing standpoint because of the number of process steps and sources required to fabricate the many layers of a conventional vacuum-deposited organic LED. These methods, while sufficient for few-color arrays, are not ideal for scaling light-emitting arrays to tens or hundreds of different colors.

Here, we address this problem by using arrays of electroluminescent, alternating current–driven metal-oxide-semiconductor (MOS) capacitors, in which the device electrodes are lithographically defined before deposition of the emitting materials (*6*). Since deposition of the emissive layer is the final fabrication step in these devices, microprinting techniques can be used to dispense many different color emitters on a single chip with ease. The rich photophysical diversity of solution-processable molecular and quantum dot materials allows for a large palette of spectral shapes to be achieved, with no modification to the device structure required for different luminescent materials. By using such an array to actively illuminate objects with spectrally varying light, spectral properties of samples can be interrogated at many wavelengths. The illuminating light spectra need not be narrowband, as optimization algorithms can be used to numerically reconstruct spectral properties of the unknown sample when using many random broadband illumination spectra. The use of compressive reconstructive methods simplifies the fabrication process since essentially any emitter with any arbitrary spectra can be used in the light-generating array. Our approach contrasts other reconstructive spectroscopic techniques that focus on modulating passive as opposed to active elements. For example, compressive spectral imaging has been demonstrated with tunable filters and many-colored filter arrays (*7*, *8*). Recent work has also shown that intrinsically or extrinsically tuned photodetectors based on nanomaterials can be used as microspectrometers to measure incident spectra in a highly compact fashion without traditional dispersive optics (e.g., diffraction gratings), heavily engineered optical components (e.g., tunable narrowband filter arrays), or bulky mechanical systems (e.g., interferometers) (*9*, *10*). These systems, in which numerical methods compensate the lack of precisely engineered components, could find use in consumer or field applications where portable, low-power devices with small footprints and costs are desirable (*11*). In this work, we illustrate how miniature arrays of electroluminescent devices with arbitrary emission spectra can be leveraged to perform active spectral measurements in a compressive manner.

RESULTS AND DISCUSSION

Electroluminescent device arrays with arbitrary spectra

Multiplexed arrays of light sources are developed using MOS capacitor devices in which emissive materials are deposited on top of capacitors fabricated on a silicon substrate (Fig. 1A and fig. S1). Alternating current voltage is applied between the two terminals of the capacitors to overcome differences in band alignment at the metal-semiconductor contact and produce transient electroluminescence (EL) at each voltage transition (Fig. 1C). The application of pulsed bias enables steep band bending and relatively efficient charge injection into different semiconducting materials from

[1]Electrical Engineering and Computer Sciences, University of California, Berkeley, Berkeley, CA 94720, USA. [2]Materials Sciences Division, Lawrence Berkeley National Laboratory, Berkeley, CA 94720, USA.
*Corresponding author. Email: ajavey@eecs.berkeley.edu

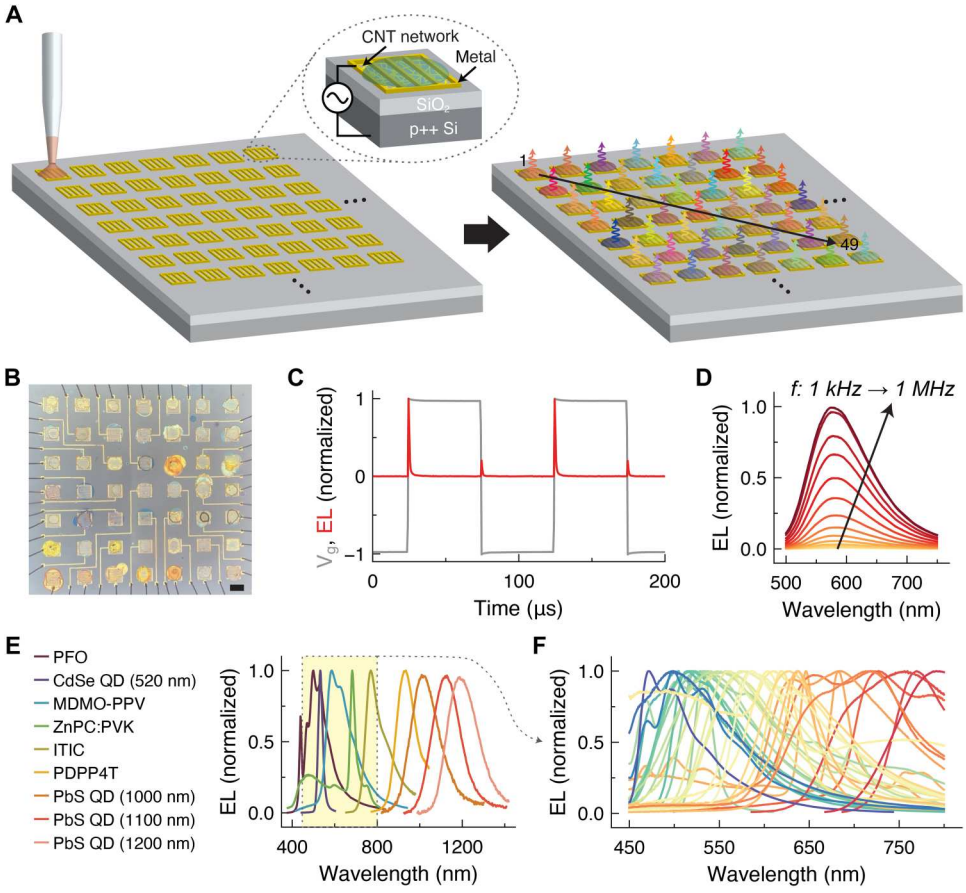

Fig. 1. Multiplexed array of multicolored electroluminescent devices. (**A**) Schematic of an array of light-emitting MOS capacitors, in which different emitting materials are microdispensed on each capacitor. (**B**) Optical image of a fabricated 7 × 7 array of devices with a different emitter dispensed on each pixel of the array. Scale bar, 400 μm. (**C**) Example of time-resolved EL (red) corresponding to a square wave pulsed gate voltage waveform (gray). (**D**) Example of increase in EL intensity with driving frequency. (**E**) EL spectra from several materials emitting across the blue to near-infrared range, with emission at all wavelengths in between. (**F**) Example of EL spectra from a wide range of materials emitting in the visible range (table S2).

metal contacts of different work functions (*12*). By using conductive carbon nanotube networks as the top source contact, a high areal density of charge carriers can be injected into materials with poor lateral charge transport (*6*, *13*). EL can be produced from materials spanning the visible to infrared range (Fig. 1E), and the intensity increases with both frequency and voltage (Fig. 1D). Figure 1F shows a dense library of emission spectra in the visible range from different material classes including organic small molecules, conjugated polymers, and colloidal quantum dots (*14*–*17*). Characterization of the brightness, efficiency, color, and spectral bandwidth of the electroluminescent devices as compared to the photoluminescence characteristics of the emitting materials is shown in figs. S2 and S3, in supplement to previous reports (*6*, *13*, *18*). The frequency response of EL from these devices depends on the resistance and capacitance of the device structure, in addition to properties of the emitting material such as radiative lifetime, of which a few examples are depicted in fig. S4 for different materials (*19*–*21*). For example, EL persists much longer after each voltage transient for a platinum octaethylporphyrin:poly(9,9-dioctyl-9H-fluorene-2,7-diyl) (PtOEP:PFO) emitter layer compared to a PFO emitter layer, in correspondence with the relatively long phosphorescence lifetime of PtOEP (*22*).

Because of the simplicity of device fabrication, large multicolor electroluminescent arrays can be fabricated on a single substrate. Figure 1B depicts an example of a 7 × 7 array of 49 light-emitting devices, in which a different emissive layer is deposited on each pixel of the array by microdispensing (fig. S5 and table S1). Nanometer film thicknesses can be obtained using this technique, corresponding to equivalent film volumes of a few picoliters (fig. S6). Notably, the bottom array of capacitors is entirely prefabricated by standard photolithography procedures, and no processing is required after deposition of the emissive layer, which reduces the complexity of device fabrication and lifts constraints on the processability of different monolithically integrated luminescent materials. The emissive layer can consist of mixtures of different materials and does not need to be thin, pinhole free, or any particular shape. The device size and pitch accuracy can be improved in the future by adopting more advanced techniques to automate the deposition of small liquid volumes [e.g., microarray printing technology, in which thousands of samples can be processed on one chip (*23*)].

To emphasize the versatility of this device platform, we first demonstrate how nearly any light spectra can be generated given a sufficiently large library of emitters. The total light spectrum from a miniature EL array is a linear combination of the spectra

from the individual elements. On the basis of this framework, an array of emitters can be designed to yield a desired light spectrum $\vec{y} = y(\lambda)$ by solving the least-squares optimization problem $\min_{\vec{\beta}} \|A\vec{\beta} - \vec{y}\|_2^2$ (subject to $\beta_j \geq 0$), where A is the set of EL spectra and $\vec{\beta}$ is the vector of linear weights for each spectrum. Since we wish to minimize the number of used spectra for practical purposes, we perform an additional initial optimization step to select a smaller subset of emitters for the array design: $\min_{\vec{\beta}} \|L\vec{\beta} - \vec{y}\|_2^2 + \gamma\|\vec{\beta}\|_1$ where L is the entire large library of EL spectra. A is then composed of the N highest-weighted spectra, where N depends on the acceptable error tolerance. The L_1 regularization term encourages sparsity in the solution and therefore reduction of N.

Figure 2 illustrates an example of spectrally matched light generation in which we targeted a spectrum that linearly varies with wavelength in the shown range. By solving the above optimization problem using a prior library of EL spectra, we found that five chosen emitters were sufficient to recreate the desired spectrum (Fig. 2, B to D, and fig. S7). The spectral weights were implemented by tuning the driving voltage and frequency for each device such that the EL intensity matched the estimated coefficient. Unlike macroscale approaches, where custom light synthesis is performed using commercial inorganic LEDs (*24*–*26*), our approach is miniaturized and compatible with spectrally diverse materials, from quantum dots with sharp emission peaks to organic polymers with broad spectral responses. This flexibility permits more accurate spectral targeting and overcomes technological limitations in the spectral availability of certain materials, such as the "green gap" from which III-nitride LEDs suffer (*27*).

Reconstructive spectral measurement

Having demonstrated the scalability and versatility of the device platform, we now show how the breadth of achievable EL spectra enables active spectral measurements. As an example, we consider the problem of measuring transmittance spectra with a single-pixel detector. The transmittance spectrum of an unknown sample is traditionally measured by passing a broadband light source through the sample, separating wavelengths of the light with a dispersive element (e.g., grating), and measuring the intensity of transmitted light with an arrayed detector. The spectral range and resolution of these systems is dictated by properties such as the grating groove density and focal length, with longer focal lengths and higher groove densities preferable for higher spectral resolution. An alternative approach to measuring spectral information, which does not require bulky engineered optical components, is reconstructive spectrometry in which spectral information can be algorithmically recovered. Figure 3A illustrates how transmittance spectra can be determined using variable incident light with arbitrary spectra and a single photodetector. By sending sufficient different but known light spectra through the sample, the transmission function of the sample can be estimated from the photodetector readings through an inverse calculation. Specifically, we solve the following optimization problem

$$\min_{\vec{c}} \|A\vec{c} - \vec{I}\|_2^2 + \gamma\|\vec{c}\|_2^2$$

$$\text{subject to } c_j \geq 0 \forall j$$

in which regularization is used to compute a solution to the underdetermined set of equations and the sample function is estimated using a set of Gaussian basis functions (*28*, *29*). A is the matrix of EL spectra (Fig. 3B) transformed by the basis functions, I is the measured photodetector values for each incident EL spectra (Fig. 3C), and $\vec{c}$ is the unknown weights of the basis functions

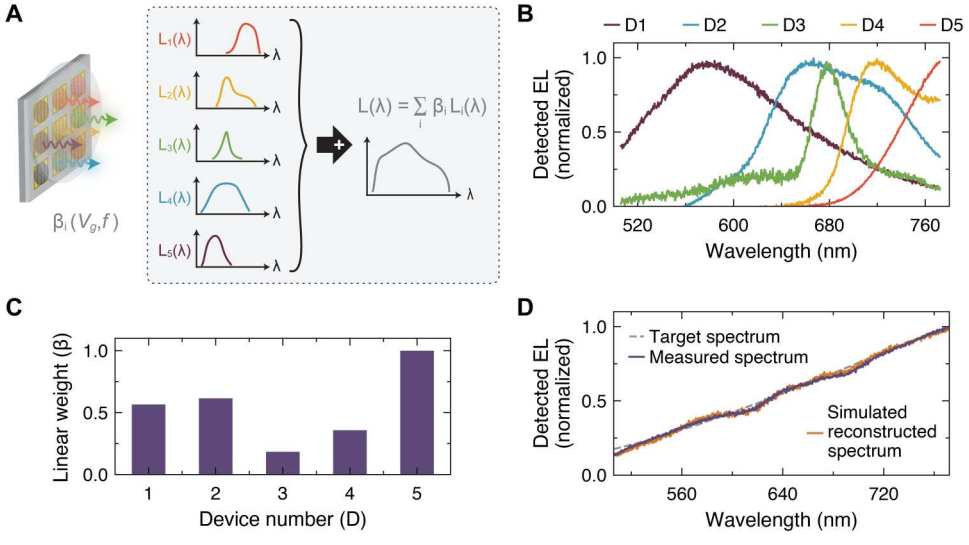

Fig. 2. Design of arbitrary EL spectra. (**A**) Schematic depicting generation of arbitrary EL spectra using an EL array. (**B**) Example of EL spectra and (**C**) relative weights of the corresponding spectra used to reconstruct the target spectrum in (**D**). The dashed gray curve represents the desired target spectrum. The purple curve represents the experimentally measured spectrum from the implemented five-device EL array. The gold curve represents the designed spectrum from calculation.

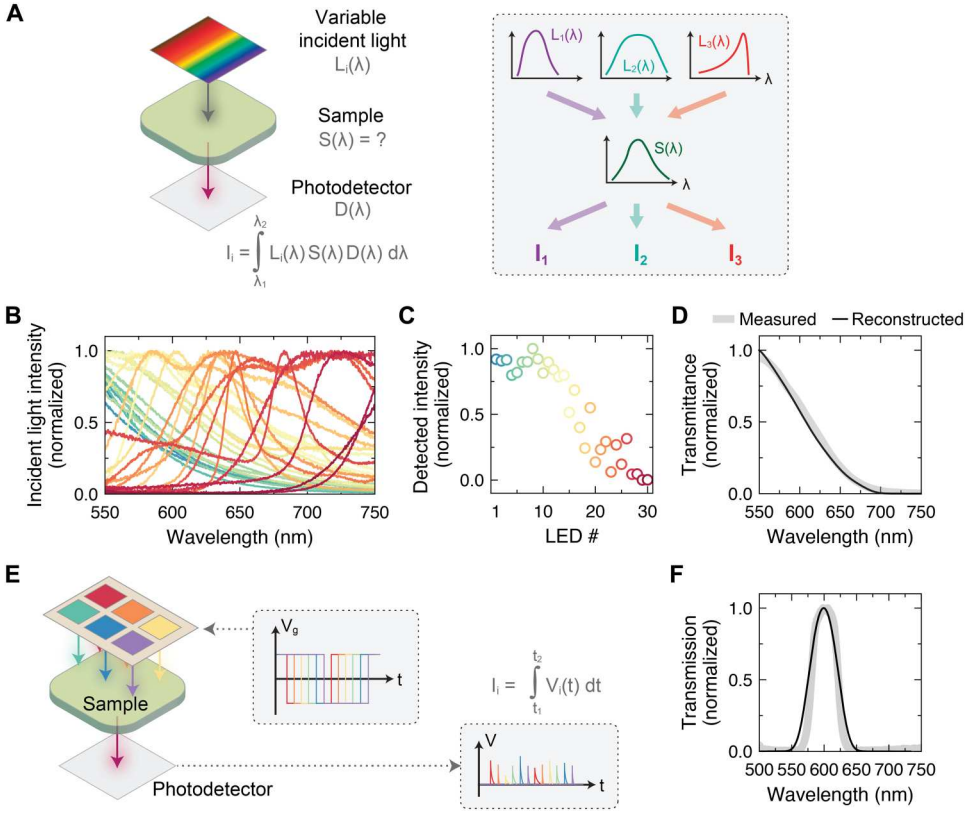

Fig. 3. Spectral measurement with highly multicolored arrays. (**A**) Schematic depicting the concept behind transmittance measurement using variable incident illumination and a single photodetector. (**B**) Spectra of EL devices (table S3) and (**C**) photodetector readings used to reconstruct the sample transmittance in (**D**). (**E**) Schematic depicting the concept behind time-multiplexed transmittance measurement using a series of phase-shifted gate voltage waveforms applied to each device in a 2 × 3 EL array. (**F**) Reconstruction of spectral transmittance based on the concept in (E).

(Supplementary Text). The result of using this scheme to measure the transmission function of a test sample is shown in Fig. 3D. The same measurement scheme can also separately distinguish two narrow band-pass filters with 10-nm spectral separation, as well as other spectral transmission functions (figs. S8 and S9). From simulated experiments of test samples with two closely spaced spectral peaks, the spectral resolution of the measurement scheme using the current set of EL spectra is estimated to be around 10 nm (fig. S10) and varies depending on the number of light-emitting devices used, with better spectral accuracy obtained as the number of measurements increases.

Because of the unique inherently pulsed nature of the devices, alternate spectral measurement schemes are possible. For example, a photodetector and lock-in amplifier can be used to perform lock-in detection of the transmitted light. This detection method enables high signal-to-noise measurement under ambient light conditions since the transmitted light is modulated at kilohertz rates and distinguishable from background lighting (fig. S11). As another example, near single-shot spectral measurement is possible using a high-speed photodetector. Each device in the array can be modulated with a different phase shift such that the light intensity from each device is distinguishable in the time-resolved capture of the photodetector readings (Fig. 3E). As a proof of concept, we fabricated a 2 × 3 array of devices and simultaneously drove each device with a square wave in which there is fixed delay between every device's applied voltage waveform (fig. S12). We then measured the time-resolved EL using a silicon photodiode, with and without the sample in between the EL array and detector (figs. S13 and S14). The transmittance spectrum of a simple unknown sample can be estimated from the known EL spectra and integrated values of time-resolved EL for each device (Fig. 3F). In principle, spectral acquisition under this scheme could be executed in as little as $N\tau$ seconds (where N is the number of devices in the array and τ is the average EL lifetime), thereby enabling fast spectral measurement without device switching.

Reconstructive spectral imaging

Last, reconstructive spectral measurements can be parallelized across space by using a detector array to perform microscopic spectral imaging. Figure 4 (A and B) illustrates measurement schemes for microscale reflected- and transmitted-light spectral imaging in which the EL array serves as the light source and a monochrome silicon charge-coupled device (CCD) camera captures images of the sample. With a single detector reading, we can only probe the micro-reflectance spectra of a single spot on a sample (several examples are shown in fig. S15), but we can reconstruct spectral reflectance at multiple spatial locations using arrayed readings from a camera. To maximize the signal and uniformly illuminate the sample, we scan each device in the EL array one at a time and capture an image of the sample under each device's illumination.

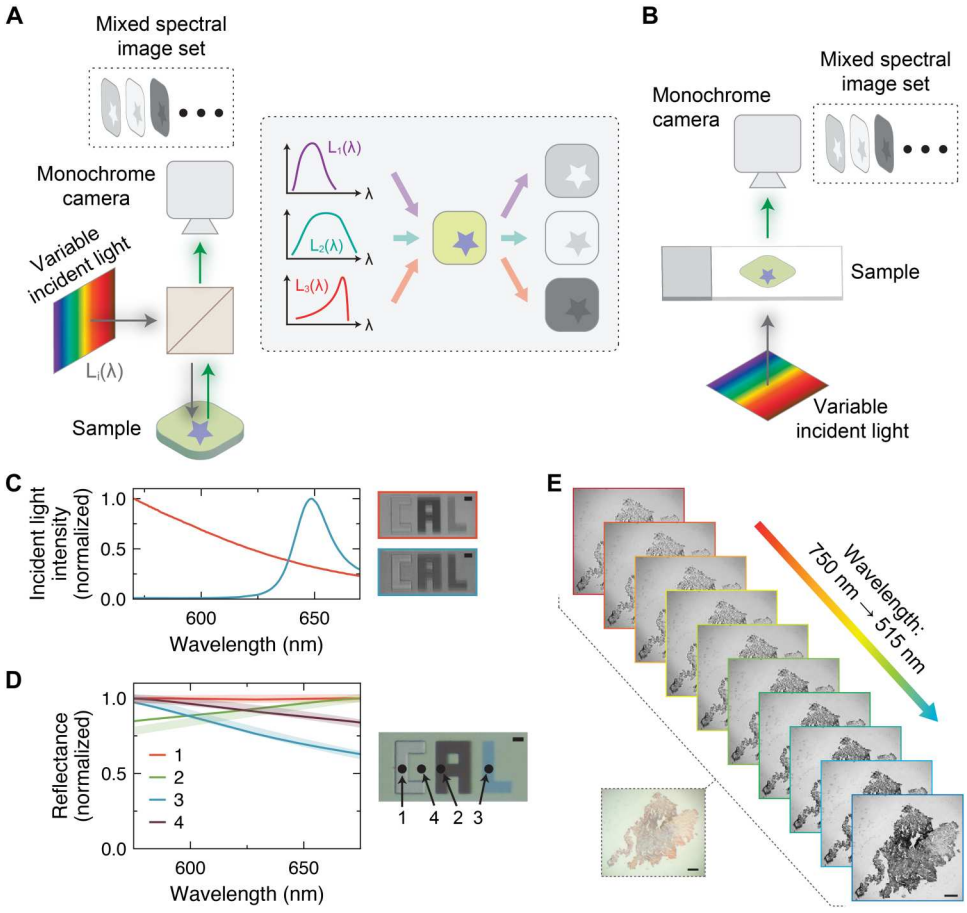

Fig. 4. Spectral imaging with highly multicolored arrays. Schematic depicting the concept behind microscale (**A**) reflected-light and (**B**) transmitted-light spectral imaging using variable incident illumination and a monochrome camera. (**C**) Example of different incident light spectra and the corresponding reflected-light microscope images. Scale bar, 40 μm. (**D**) Reconstructed reflectance spectra at different spots on the sample shown in the optical micrograph, using the emitters in table S4. Scale bar, 40 μm. (**E**) Spectral data cube for a human tissue sample imaged using a transmitted-light imaging setup. Scale bars, 100 μm.

We then decode the spectral response at each pixel using the reconstruction algorithm described earlier. Figure 4 (C and D) shows an example of reflected-light imaging of a thin-film sample where different colors correspond to different thicknesses of silicon dioxide on a silicon substrate. When the sample is illuminated by different devices, different grayscale images are captured (Fig. 4C) and these data are used to reconstruct the reflectance spectra in different regions (Fig. 4D). The obtained spectra closely match the simulated reflectance spectra for this thin-film stack based on transfer matrix method calculations and atomic force microscopy (AFM) measurements of the oxide thicknesses (fig. S16). Spectral imaging of semitransparent biological samples (in this case, a stained human tissue slice) can be performed in a transmitted-light configuration, from which we extract the deconvolved spectral image set displayed in Fig. 4E. A summary of different reconstructive spectral imaging approaches can be found in table S5. Compared to reconstructive microscale spectral imaging approaches that rely on the modulation of passive elements such as a single tuned photodetector, modulation of the active illumination enables faster acquisition of spectral image stacks with larger image sizes due to its compatibility with standard microscopes, which avoids the need for time-intensive spatial scanning. Similarly, our approach does not rely on modification of or adaptation of the spectral element to the camera or image sensor (*30*–*32*). Because light emission can be generated across a broad spectral range, the potentially achievable spectral range is broader and does not rely on carefully engineered material syntheses or highly material-specific physics (*9*, *33*, *34*).

Multiplexed illumination has been previously explored as an approach toward multispectral imaging at the macroscale (*35*, *36*); however, the methodology made use of only a handful of LEDs due to limited commercial availability of different wavelength light sources. Compressive approaches toward active illumination-based spectral imaging have also been developed using macroscale assemblies of commercial LEDs (*37*–*39*), and concepts from these works may complement the development of new spectral imaging approaches based on a highly multispectral light-emitting capacitor array, for which the generic nature of the light emission mechanism enables spectral sensing across a broad photon energy range. The ability to miniaturize the light-emitting array to nano- or microscale dimensions on a single substrate could further enable chip-scale operation of applications necessitating many spectral bands. In the future, design procedures for the selection of optimal electroluminescent spectra for different applications could be developed on the basis of principles from compressive sensing theory (*40*). For

example, using a series of linearly spaced Gaussian emission spectra may yield smaller reconstruction error for a broadband spectral reconstruction task than using the happenstance matrix of EL colors presented here (fig. S17). By using an illumination basis set with less correlated spectra, lower reconstruction error and higher spectral accuracy could be achieved with a fewer number of light sources. It may also be possible to design an adaptive sensing scheme in which light-emitting sources are dynamically chosen on the basis of preceding measurements to optimize the number and sequence of measurements.

In summary, we have developed a simple and scalable means of creating monolithic light-emitting device arrays with highly multiplexed emission spanning the visible to infrared wavelength range. By using pulsed-driven MOS capacitors, we can achieve bipolar charge injection and bright EL without relying on emitter-specific injection or transport layers, which complicate the integration of multicolor devices. Our platform can be used as a source of variable and arbitrary light emission with which to probe the spectral properties of samples, where here we show spectral reflectance and transmittance imaging as an example. Spectral accuracy and coverage could be improved by using spectrally tuned materials instead of arbitrary commercially available materials. Examples include colloidal quantum dot and perovskite nanomaterials, in which narrowband emission spectra at different wavelengths can be achieved by tuning the size and alloy composition (*41*–*43*), or thin luminescent films fabricated by combinatorial deposition, in which materials with tunable emission might be achieved in a single step (*44*). While we focus on the visible spectrum in this work, this concept can be extended to more extreme wavelengths by exploring other materials (*6*). A virtually infinite number of different colors can be achieved on any length scale since lithographic patterning of the devices allows for the fabrication of large arrays and small light-emitting pixel sizes. More advanced machine learning algorithms may further improve the fidelity of spectral reconstruction (*45*, *46*). Since pixels in the light-emitting array can be addressed individually or collectively, light can be generated with customizable patterns in frequency, space, and time, offering an avenue toward active spectral measurements across multiple dimensions.

MATERIALS AND METHODS

Device fabrication

The fabrication of carbon nanotube MOS capacitors follows a procedure previously described in the literature (*47*). To summarize, clean 90-nm SiO_2/p++ Si substrates are treated with O_2 plasma for 1.5 min. Poly-L-lysine solution (0.1%, w/v, aqueous solution, Ted Pella) is drop-cast on the substrate for 5 min and then rinsed off with deionized (DI) water. Ninety percent semiconducting single-walled carbon nanotube (SWNT) solution (IsoNanotubes-S, NanoIntegris) is drop-cast on the substrate for 10 min and then rinsed off with DI water. The substrate is subsequently annealed in forming gas for 1 hour at 250°C. Metal contacts are patterned by photolithography and deposited by e-beam evaporation of Ti (5 nm)/Au (30 nm). The active device areas are patterned by photolithography, and SWNTs outside the device areas are etched by O_2 plasma.

Emitters are dispensed on the devices using glass micropipettes, which are fabricated using a micropipette puller (P-30, Sutter Instrument) and thin-wall borosilicate glass capillaries with 1-mm outer diameter (B100-75-10, Sutter Instrument or TW100-4, World Precision Instruments). Emissive materials, which include organic molecules and quantum dots in this work, are dispensed from solution with a typical concentration around 5 to 10 mg/ml in chlorobenzene or toluene, except for ionic transition-metal complexes, which are dissolved in acetonitrile. Organic small-molecule emitters and metal phthalocyanines are diluted as dopants in a poly(9-vinylcarbazole) (PVK) polymer host at a relative weight concentration of typically a few percent, except for PtOEP and pentacene, which are dispersed in PFO (*22*, *48*). Refer to table S1 for more details. Materials are obtained from Sigma-Aldrich [520- and 600-nm CdSe/ZnS quantum dots in toluene, 525- and 630-nm CdSeS/ZnS alloyed quantum dots in toluene, 9,10-diphenylanthracene, 4CzIPN, rubrene, $Ir(ppy)_3$, $Ru(bpy)_3(PF_6)_2$, $Ru(p\text{-}CF_3\text{-}bpy)_3(BF_4)_2$, $Ir(dtb\text{-}bpy)(ppy)_2PF_6$, $Ir(dF\text{-}ppy)_2(dtb\text{-}bpy)]PF_6$, zinc phthalocyanine, titanyl phthalocyanine, MDMO-PPV, PFV, PDY-132, PFO, PVK, and 1000-nm PbS quantum dots in toluene]; Luminescence Technology Corp. [$Ir(ppy)_2(acac)$, CzDBA, PtOEP, Alq_3, F8BT, MEH-PPV, FIrPic, CBP, and pentacene]; Quantum Solutions [1100- and 1200-nm PbS quantum dots, dissolved in toluene]; Ossila (PDPP4T); Strem [$Ir(Fppy)_3$], 1-Material (P3HT; Y6); Solaris Chem (PTB7); Nano-C (C60-PCBM); and Brilliant Matters (ITIC; PBDB-T).

Sample fabrication

The "CAL" sample for reflected-light imaging is fabricated from 500-nm SiO_2/Si substrate. The substrate is first immersed in 6:1 buffered oxide etch (HF) until the desired oxide thickness is achieved and then rinsed with DI water and dried. Three successive rounds of photolithography are performed using a direct-write tool (Heidelberg μPG 101) to pattern each of the letters. After each photolithography step, the substrate is immersed in 6:1 buffered oxide etch until the desired oxide thickness is achieved and then rinsed with DI water and dried. The remaining photoresist is removed with Remover PG before continuing onto the next photolithography step. The etch rates and oxide thicknesses are calibrated and validated by AFM measurement.

Device measurement

To drive the devices, pulsed electrical bias is applied using a function generator (33522A, Agilent) and voltage amplifier, where multiplexing is implemented with a commercial board (EL Escudo Dos, SparkFun) or solid-state relays. A custom-built square wave generating circuit controlled by an Arduino microcontroller is used for phase shift multiplexed measurements (fig. S12). Optical measurements, including direct measurement of EL, reflectance, and transmittance spectra, are performed using a custom-built microphotoluminescence setup, in which EL can be collected by a photodiode and a camera or dispersed by a spectrograph (HR-640, Instruments SA) with a 150 groove/mm grating and detected by a Si CCD (iDus BEX2-DD, Andor) (*49*). For each measurement, the dark background of the CCD is measured and subtracted from the acquired signal. The instrument sensitivity as a function of wavelength is determined by measuring the response of a Lambertian light source generated by illumination from a temperature-stabilized lamp (SLS201, ThorLabs) on a diffuse reflector (Spectralon). Reflected-light spectral imaging is performed using the same fluorescence microscopy setup, while transmitted-light spectral imaging is performed using a separate custom-built microscope

(Cerna Microscopy Platform, ThorLabs), in which illumination from the EL array is defocused at the sample. Imaging measurements are acquired with a CCD camera (Luca-R, Andor). A silver mirror and glass microscope slide (on part of which the tissue sample in Fig. 4 is mounted) are used as references for calibrating spectral reflectance and transmittance. Low-pass and high-pass filters were included in the optical path to define the spectral range in the reconstruction experiments to the wavelength limits shown. Time-resolved EL measurements are acquired using a Si photodetector (APD410A, ThorLabs) and oscilloscope (TDS-640A, Tektronix), and time-averaged measurements are acquired using the same detector with a lock-in amplifier (SRS-830, Stanford Research Systems). Devices are operated under vacuum at room temperature. A diffuser is placed above the device array when measuring composite EL spectra. Hardware control and data acquisition are performed using custom Python software based on the open-source ScopeFoundry platform. Data are analyzed in Python using the cvxpy package for numerical optimization.

Supplementary Materials

This PDF file includes:

Figs. S1 to S17
Tables S1 to S5
Supplementary Text

REFERENCES AND NOTES

1. P. M. Pattison, J. Y. Tsao, G. C. Brainard, B. Bugbee, LEDs for photons, physiology and food. *Nature* **563**, 493–500 (2018).
2. T. Wang, S.-Y. Ma, L. G. Wright, T. Onodera, B. C. Richard, P. L. McMahon, An optical neural network using less than 1 photon per multiplication. *Nat. Commun.* **13**, 123 (2022).
3. C. P. Bacon, Y. Mattley, R. DeFrece, Miniature spectroscopic instrumentation: Applications to biology and chemistry. *Rev. Sci. Instrum.* **75**, 1–16 (2004).
4. C. D. Müller, A. Falcou, N. Reckefuss, M. Rojahn, V. Wiederhirn, P. Rudati, H. Frohne, O. Nuyken, H. Becker, K. Meerholz, Multi-colour organic light-emitting displays by solution processing. *Nature* **421**, 829–833 (2003).
5. C.-Z. Ning, L. Dou, P. Yang, Bandgap engineering in semiconductor alloy nanomaterials with widely tunable compositions. *Nat. Rev. Mater.* **2**, 1–14 (2017).
6. Y. Zhao, V. Wang, D.-H. Lien, A. Javey, A generic electroluminescent device for emission from infrared to ultraviolet wavelengths. *Nat. Electron.* **3**, 612–621 (2020).
7. X. Wang, Y. Zhang, X. Ma, T. Xu, G. R. Arce, Compressive spectral imaging system based on liquid crystal tunable filter. *Opt. Express* **26**, 25226–25243 (2018).
8. J. Bao, M. G. Bawendi, A colloidal quantum dot spectrometer. *Nature* **523**, 67–70 (2015).
9. Z. Yang, T. Albrow-Owen, H. Cui, J. Alexander-Webber, F. Gu, X. Wang, T. C. Wu, M. Zhuge, C. Williams, P. Wang, A. V. Zayats, W. Cai, L. Dai, S. Hofmann, M. Overend, L. Tong, Q. Yang, Z. Sun, T. Hasan, Single-nanowire spectrometers. *Science* **365**, 1017–1020 (2019).
10. S. Yuan, D. Naveh, K. Watanabe, T. Taniguchi, F. Xia, A wavelength-scale black phosphorus spectrometer. *Nat. Photonics* **15**, 601–607 (2021).
11. Z. Yang, T. Albrow-Owen, W. Cai, T. Hasan, Miniaturization of optical spectrometers. *Science* **371**, eabe0722 (2021).
12. D.-H. Lien, M. Amani, S. B. Desai, G. H. Ahn, K. Han, J.-H. He, J. W. Ager III, M. C. Wu, A. Javey, Large-area and bright pulsed electroluminescence in monolayer semiconductors. *Nat. Commun.* **9**, 1229 (2018).
13. V. Wang, Y. Zhao, A. Javey, Performance limits of an alternating current electroluminescent device. *Adv. Mater.* **33**, e2005635 (2021).
14. T. H. Han, M. R. Choi, C. W. Jeon, Y. H. Kim, S. K. Kwon, T. W. Lee, Ultrahigh-efficiency solution-processed simplified small-molecule organic light-emitting diodes using universal host materials. *Sci. Adv.* **2**, e1601428 (2016).
15. H. Zheng, Y. Zheng, N. Liu, N. Ai, Q. Wang, S. Wu, J. Zhou, D. Hu, S. Yu, S. Han, W. Xu, C. Luo, Y. Meng, Z. Jiang, Y. Chen, D. Li, F. Huang, J. Wang, J. Peng, Y. Cao, All-solution processed polymer light-emitting diode displays. *Nat. Commun.* **4**, 1971 (2013).
16. R. D. Costa, E. Ortí, H. J. Bolink, F. Monti, G. Accorsi, N. Armaroli, Luminescent ionic transition-metal complexes for light-emitting electrochemical cells. *Angew. Chem. Int. Ed.* **51**, 8178–8211 (2012).
17. Y. Shirasaki, G. J. Supran, M. G. Bawendi, V. Bulović, Emergence of colloidal quantum-dot light-emitting technologies. *Nat. Photonics* **7**, 13–23 (2013).
18. V. Wang, A. Javey, A resonantly driven, electroluminescent metal oxide semiconductor capacitor with high power efficiency. *ACS Nano* **15**, 15210–15217 (2021).
19. J. D. Slinker, A. A. Gorodetsky, M. S. Lowry, J. Wang, S. Parker, R. Rohl, S. Bernhard, G. G. Malliaras, Efficient yellow electroluminescence from a single layer of a cyclometalated iridium complex. *J. Am. Chem. Soc.* **126**, 2763–2767 (2004).
20. A. P. Kulkarni, X. Kong, S. A. Jenekhe, Fluorenone-containing polyfluorenes and oligofluorenes: Photophysics, origin of the green emission and efficient green electroluminescence. *J. Phys. Chem. B* **108**, 8689–8701 (2004).
21. I. Rörich, O. V. Mikhnenko, D. Gehrig, P. W. M. Blom, N. I. Crăciun, Influence of energetic disorder on exciton lifetime and photoluminescence efficiency in conjugated polymers. *J. Phys. Chem. B* **121**, 1405–1412 (2017).
22. P. A. Lane, L. C. Palilis, D. F. O'Brien, C. Giebeler, A. J. Cadby, D. G. Lidzey, A. J. Campbell, W. Blau, D. D. C. Bradley, Origin of electrophosphorescence from a doped polymer light emitting diode. *Phys. Rev. B* **63**, 235206 (2001).
23. R. L. Stears, T. Martinsky, M. Schena, Trends in microarray analysis. *Nat. Med.* **9**, 140–145 (2003).
24. F. Zhang, H. Xu, Z. Wang, Spectral design methods for multi-channel LED light sources based on differential evolution. *Appl. Optics* **55**, 7771–7781 (2016).
25. G. Belušič, M. Ilić, A. Meglič, P. Pirih, A fast multispectral light synthesiser based on LEDs and a diffraction grating. *Sci. Rep.* **6**, 32012 (2016).
26. K. Franke, A. M. Chagas, Z. Zhao, M. J. Y. Zimmermann, P. Bartel, Y. Qiu, K. P. Szatko, T. Baden, T. Euler, An arbitrary-spectrum spatial visual stimulator for vision research. *eLife* **8**, e48779 (2019).
27. A. David, N. G. Young, C. A. Hurni, M. D. Craven, Quantum efficiency of III-nitride emitters: Evidence for defect-assisted nonradiative recombination and its effect on the green gap. *Phys. Rev. Appl.* **11**, 031001 (2019).
28. R. M. H. Nguyen, D. K. Prasad, M. S. Brown, Training-based spectral reconstruction from a single RGB image, in *European Conference on Computer Vision* (Springer International Publishing, 2014), pp. 186–201.
29. U. Kurokawa, B. I. Choi, C.-C. Chang, Filter-based miniature spectrometers: Spectrum reconstruction using adaptive regularization. *IEEE Sens. J.* **11**, 1556–1563 (2011).
30. Z. Wang, S. Yi, A. Chen, M. Zhou, T. S. Luk, A. James, J. Nogan, W. Ross, G. Joe, A. Shahsafi, K. X. Wang, M. A. Kats, Z. Yu, Single-shot on-chip spectral sensors based on photonic crystal slabs. *Nat. Commun.* **10**, 1020 (2019).
31. M. Yako, Y. Yamaoka, T. Kiyohara, C. Hosokawa, A. Noda, K. Tack, N. Spooren, T. Hirasawa, A. Ishikawa, Video-rate hyperspectral camera based on a CMOS-compatible random array of Fabry–Pérot filters. *Nat. Photonics* **17**, 218–223 (2023).
32. W. Zhang, H. Song, X. He, L. Huang, X. Zhang, J. Zheng, W. Shen, X. Hao, X. Liu, Deeply learned broadband encoding stochastic hyperspectral imaging. *Light Sci. Appl.* **10**, 108 (2021).
33. H. H. Yoon, H. A. Fernandez, F. Nigmatulin, W. Cai, Z. Yang, H. Cui, F. Ahmed, X. Cui, M. G. Uddin, E. D. Minot, H. Lipsanen, K. Kim, P. Hakonen, T. Hasan, Z. Sun, Miniaturized spectrometers with a tunable van der Waals junction. *Science* **378**, 296–299 (2022).
34. W. Deng, Z. Zheng, J. Li, R. Zhou, X. Chen, D. Zhang, Y. Lu, C. Wang, C. You, S. Li, L. Sun, Y. Wu, X. Li, B. An, Z. Liu, Q. J. Wang, X. Duan, Y. Zhang, Electrically tunable two-dimensional heterojunctions for miniaturized near-infrared spectrometers. *Nat. Commun.* **13**, 4627 (2022).
35. J. Il Park, M. H. Lee, M. D. Grossberg, S. K. Nayar, Multispectral imaging using multiplexed illumination, in *2007 IEEE 11th International Conference on Computer Vision* (IEEE, 2007), pp. 1–8.
36. M. Goel, E. Whitmire, A. Mariakakis, T. S. Saponas, N. Joshi, D. Morris, B. Guenter, M. Gavriliu, G. Borriello, S. N. Patel, HyperCam: Hyperspectral imaging for ubiquitous computing applications, in *Proceedings of the 2015 ACM International Joint Conference on Pervasive and Ubiquitous Computing*, *UbiComp '15* (Association for Computing Machinery, 2015), pp. 145–156.
37. X. Ma, X. Yuan, C. Fu, G. R. Arce, Active illumination compressive 4D spectral video imaging system, in *OSA Imaging and Applied Optics Congress 2021* (Optica Publishing Group, 2021).
38. X. Ma, X. Yuan, C. Fu, G. R. Arce, LED-based compressive spectral-temporal imaging. *Opt. Express* **29**, 10698–10715 (2021).
39. A. Wagadarikar, R. John, R. Willett, D. Brady, Single disperser design for coded aperture snapshot spectral imaging. *Appl. Optics* **47**, B44–B51 (2008).
40. G. R. Arce, D. J. Brady, L. Carin, H. Arguello, D. S. Kittle, Compressive coded aperture spectral imaging: An introduction. *IEEE Signal Process. Mag.* **31**, 105–115 (2014).
41. P. O. Anikeeva, J. E. Halpert, M. G. Bawendi, V. Bulović, Quantum dot light-emitting devices with electroluminescence tunable over the entire visible spectrum. *Nano Lett.* **9**, 2532–2536 (2009).

42. I. Moreels, Y. Justo, B. De Geyter, K. Haustraete, J. C. Martins, Z. Hens, Size-tunable, bright, and stable PbS quantum dots: A surface chemistry study. *ACS Nano* **5**, 2004–2012 (2011).
43. I. Levchuk, A. Osvet, X. Tang, M. Brandl, J. D. Perea, F. Hoegl, G. J. Matt, R. Hock, M. Batentschuk, C. J. Brabec, Brightly luminescent and color-tunable formamidinium lead halide perovskite FAPbX3 (X = Cl, Br, I) colloidal nanocrystals. *Nano Lett.* **17**, 2765–2770 (2017).
44. E. Danielson, J. H. Golden, E. W. McFarland, C. M. Reaves, W. H. Weinberg, X. D. Wu, A combinatorial approach to the discovery and optimization of luminescent materials. *Nature* **389**, 944–948 (1997).
45. L. Huang, R. Luo, X. Liu, X. Hao, Spectral imaging with deep learning. *Light Sci. Appl.* **11**, 61 (2022).
46. Y. Fu, Y. Zou, Y. Zheng, H. Huang, Spectral reflectance recovery using optimal illuminations. *Opt. Express* **27**, 30502–30516 (2019).
47. C. Wang, D. Hwang, Z. Yu, K. Takei, J. Park, T. Chen, B. Ma, A. Javey, User-interactive electronic skin for instantaneous pressure visualization. *Nat. Mater.* **12**, 899–904 (2013).
48. C.-L. Lee, K. B. Lee, J.-J. Kim, Polymer phosphorescent light-emitting devices doped with tris(2-phenylpyridine) iridium as a triplet emitter. *Appl. Phys. Lett.* **77**, 2280–2282 (2000).
49. M. Amani, D. H. Lien, D. Kiriya, J. Xiao, A. Azcatl, J. Noh, S. R. Madhvapathy, R. Addou, K. C. Santosh, M. Dubey, K. Cho, R. M. Wallace, S. C. Lee, J. H. He, J. W. Ager, X. Zhang, E. Yablonovitch, A. Javey, Near-unity photoluminescence quantum yield in MoS_2. *Science* **350**, 1065–1068 (2015).

Acknowledgments: We thank J. Kim for helpful discussions and E. Chan for providing quantum dot samples from the Molecular Foundry at Lawrence Berkeley National Laboratory. **Funding:** This work was funded by the U.S. Department of Energy, Office of Science, Office of Basic Energy Sciences, Materials Sciences and Engineering Division under contract no. DE-AC02-05-CH11231 (EMAT program KC1201). Device processing was partly supported by Samsung.
Author contributions: V.W. and A.J. conceived the idea for the project. V.W. and S.Z.U. designed and constructed the experimental methods. V.W. and J.P. fabricated devices. V.W. performed the experiments, analyzed the data, and wrote the manuscript. All authors commented on the results and manuscript. **Competing interests:** The authors declare that they have no competing interests. **Data and materials availability:** All data needed to evaluate the conclusions in the paper are present in the paper and/or the Supplementary Materials.

Submitted 6 December 2022
Accepted 16 March 2023
Published 19 April 2023
10.1126/sciadv.adg1607